



Electronic structure of the bond disproportionated bismuthate Ag_2BiO_3

Mohamed Oudah,^{1,2,*} Minu Kim,¹ Ksenia S. Rabinovich,¹ Kateryna Foyevtsova,² Graham McNally,¹ Berkay Kilic ,¹ Kathrin Küster,¹ Robert Green,^{2,3} Alexander V. Boris ,¹ George Sawatzky,² Andreas P. Schnyder,¹ D. A. Bonn,² Bernhard Keimer,¹ and Hidenori Takagi^{1,4}

¹Max Planck Institute for Solid State Research, Heisenbergstrasse 1, 70569 Stuttgart, Germany

²Stewart Blusson Quantum Matter Institute, University of British Columbia, Vancouver, British Columbia V6T 1Z4, Canada

³Department of Physics & Engineering Physics, University of Saskatchewan, Saskatoon, Saskatchewan S7N 5E2, Canada

⁴Department of Physics, University of Tokyo, Bunkyo-ku, Hongo 7-3-1, Tokyo 113-0033, Japan



(Received 15 September 2020; accepted 14 June 2021; published 24 June 2021)

We present a comprehensive study on the silver bismuthate Ag_2BiO_3 , synthesized under high-pressure, high-temperature conditions, which has been the subject of recent theoretical work on topologically complex electronic states. We present x-ray photoelectron spectroscopy results showing two different bismuth states and x-ray absorption spectroscopy results on the oxygen K edge showing holes in the oxygen bands. These results support a bond disproportionated state with holes on the oxygen atoms for Ag_2BiO_3 . We estimate a band gap of ~ 1.25 eV for Ag_2BiO_3 from optical conductivity measurements, which matches the band gap in density functional calculations of the electronic band structure in the nonsymmorphic space group $Pnn2$, which supports two inequivalent Bi sites. In our band structure calculations the disproportionated Ag_2BiO_3 is expected to host Weyl nodal chains, one of which is located ~ 0.5 eV below the Fermi level. Furthermore, we highlight similarities between Ag_2BiO_3 and the well-known disproportionated bismuthate BaBiO_3 , including breathing phonon modes with similar energy. In both compounds, hybridization of Bi $6s$ and O $2p$ atomic orbitals is important in shaping the band structure, but in contrast to the Ba $5p$ bands in BaBiO_3 , the Ag $4d$ bands in Ag_2BiO_3 extend up to the Fermi level.

DOI: [10.1103/PhysRevMaterials.5.064202](https://doi.org/10.1103/PhysRevMaterials.5.064202)

I. INTRODUCTION

Transition-metal oxides include many novel classes of materials that host a wide range of structures and electronic properties. The field of condensed matter physics had made a great leap forward with the discovery of high-transition-temperature superconductivity (T_c) in the layered copper oxides [1] and in the hole-doped cubic bismuthate $(\text{Ba,K})\text{BiO}_3$ [2]. The undoped BaBiO_3 is a disproportionated insulator. Also, oxide materials have shown promise for exploring topological properties [3–5]. We identified the silver bismuthates as a promising set of materials for studying highly correlated electron systems and for finding topologically nontrivial oxides. Ag_2BiO_3 was recently highlighted in theoretical work with various predictions of topologically protected states [6–8].

The previous experimental work on Ag_2BiO_3 has resulted in a number of crystal structures reported in the Inorganic Crystal Structure Database (ICSD), which fall into the space

groups $Pnna$, $Pnn2$, and Pn [9,10]. $Pnna$ is the oldest structure reported, which has a single bismuth site implying a uniform $4+$ state for bismuth and as a result equal Bi-O distances. A Bi^{4+} state is unusual, however, and typically a compound with nominal charge of $4+$ on bismuth disproportionates. The disproportionation in BaBiO_3 is reflected in the existence of two distinct sites for Bi, but the nature of this disproportionation is debated. It was emphasized in a following neutron diffraction study that Ag_2BiO_3 has two distinct bismuth sites and crystallizes in the $Pnn2$ space group [10], and the two sites were explained with the disproportionation of Bi^{4+} into Bi^{3+} and Bi^{5+} states. The existence of two distinct bismuth sites in Ag_2BiO_3 ($Pnn2$) is similar to BaBiO_3 , but these compounds crystallize in different crystal structures, with a combination of corner- and edge-sharing BiO_6 octahedra in Ag_2BiO_3 and only corner-sharing BiO_6 octahedra in the perovskite BaBiO_3 (Fig. 1). By thoroughly characterizing the disproportionated state in Ag_2BiO_3 and comparing with BaBiO_3 , we establish $(M^{1+})_2\text{BiO}_3$ as a class of disproportionated bismuthates beyond those forming in the perovskite structure.

The disproportionation of the Bi site and resulting $Pnn2$ symmetry also have important ramifications for the topological nature of Ag_2BiO_3 . Theoretical predictions of topological phases in Ag_2BiO_3 include an hourglass nodal net semimetal [7], a Dirac semimetal [6], and an hourglass Dirac semimetal [8]. All of these topological predictions were made on Ag_2BiO_3 in the $Pnna$ phase with a single bismuth site,

*mohamed.oudah@ubc.ca

Published by the American Physical Society under the terms of the Creative Commons Attribution 4.0 International license. Further distribution of this work must maintain attribution to the author(s) and the published article's title, journal citation, and DOI. Open access publication funded by the Max Planck Society.

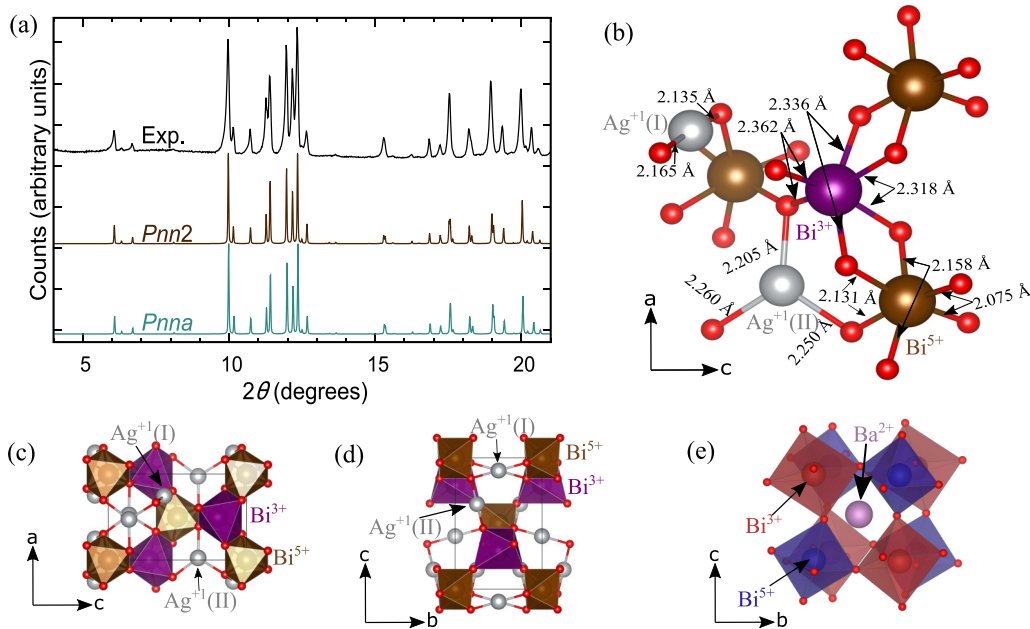


FIG. 1. (a) The powder x-ray diffraction pattern measured at room temperature of Ag_2BiO_3 (top) and the calculated pattern for Ag_2BiO_3 in the $Pnn2$ phase (middle) and the $Pnna$ phase (bottom). (b) Part of the unit cell of Ag_2BiO_3 in the $Pnn2$ phase with “ Bi^{3+} ” (purple) and “ Bi^{5+} ” (brown) highlighting the different oxygen metal distances [10]. (c) Unit cell of Ag_2BiO_3 in the $Pnn2$ phase along the ac plane showing the shared edges of the octahedra along the a direction. (d) Unit cell of Ag_2BiO_3 in the $Pnn2$ phase along the bc plane. (e) Unit cell of BaBiO_3 showing the corner-sharing octahedra and Bi^{3+} (red) and Bi^{5+} (blue).

where breaking Bi charge order to attain the $Pnna$ symmetry is important to realizing these topologically nontrivial phases. However, we will show that Ag_2BiO_3 crystallizes in the $Pnn2$ space group with two crystallographically distinct bismuth sites even when synthesized under high-pressure and high-temperature conditions. The topological predictions made for the $Pnna$ phase therefore do not apply to Ag_2BiO_3 crystallizing in the $Pnn2$ phase. Rather, we predict Weyl states in the $Pnn2$ phase.

In this paper, we characterize Ag_2BiO_3 samples synthesized at 6 GPa using powder x-ray diffraction (XRD) and various spectroscopic techniques. We present evidence from x-ray photoelectron spectroscopy (XPS) supporting the disproportionation of bismuth into two sites in Ag_2BiO_3 and present evidence for a bulk band gap, a consequence of the disproportionation, seen in an optical conductivity measurement. The optical gap is consistent with density functional theory (DFT) calculations of the electronic band structure in the $Pnn2$ (disproportionated) phase of this material. Our calculations, on the experimentally realized $Pnn2$ phase, further predict Weyl nodal chains (i.e., chains of connected loop degeneracies in momentum space) at various energies in this phase, one being ~ 0.5 eV below the Fermi level. We provide evidence for oxygen holes using x-ray absorption spectroscopy (XAS), and considering the XPS results, we propose that Ag_2BiO_3 is bond disproportionated rather than charge disproportionated. We then highlight the extent of similarities between Ag_2BiO_3 and BaBiO_3 ; similar breathing mode peaks are observed in Raman spectra, and we identify similarities in the band structure of these compounds when considering the oxygen molecular orbitals in these disproportionated bismuthates. Finally, we present evidence from

Raman spectra and XRD for the previously reported structural transition to a Pn phase at low temperature [10].

II. EXPERIMENTAL DETAILS

Ag_2BiO_3 samples were synthesized with a high-pressure, high-temperature method utilizing a belt press. Bi_2O_3 and AgO powders were well mixed with a mortar and pestle and then loaded into a gold capsule with a drop of KOH to speed up the reaction. The capsule was then pressed to 6 GPa and heated at 730 K for 1 h before quenching and retrieving the polycrystalline product. A finely ground sample was loaded into a 0.3-mm capillary, and powder XRD patterns of Ag_2BiO_3 were collected while rotating the capillary using Ag radiation (0.5594 Å). The samples were cooled down to ~ 200 K for low-temperature XRD.

X-ray absorption spectra of the oxygen K edges were recorded in partial fluorescence yield (PFY) mode at the spherical-grating monochromator (SGM) beamline at the Canadian Light Source. Spectra in PFY mode are collected using energy-resolving silicon drift detectors, which allow selection of only the oxygen K -edge fluorescence. The average of data from four separate silicon drift detectors was used for the PFY spectra. Spectra are calibrated in energy by using a TiO_2 reference sample [11]. Spectra were then normalized by the incident beam intensity and normalized according to postedge intensity after subtracting a linear background. The Ag_2BiO_3 spectra were collected under ultrahigh vacuum at room temperature from a pressed pellet attached to carbon tape, with the pellet surface at an angle of 45° to the incident beam. The XPS data were collected using a commercial Kratos AXIS Ultra spectrometer and a monochromatized Al

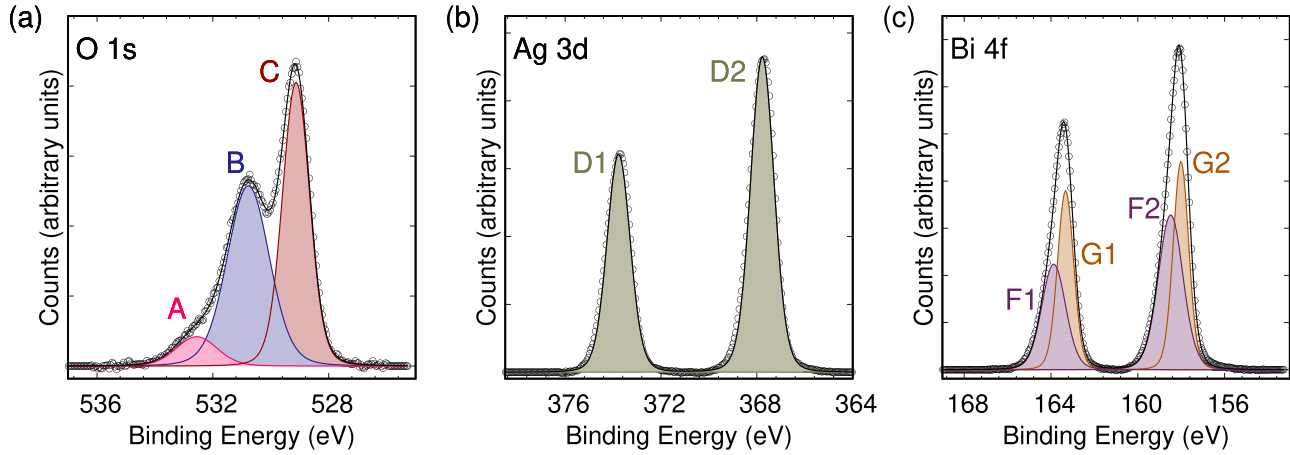


FIG. 2. X-ray photoelectron spectra of O, Ag, and Bi in Ag_2BiO_3 are shown in (a), (b), and (c), respectively. In (a) the three peaks A, B, and C are needed to fit the measured spectra for the O $1s$ states. In (b) the splitting between peaks D1 and D2 is consistent with that expected due to spin-orbit coupling (SOC) for Ag $3d$ states. In (c) the splitting between F1 and F2 is consistent with that expected due to SOC for Bi $4f$ states, and the same can be said for the split between G1 and G2. Due to the asymmetry of the measured spectra, four curves are needed to fit the Bi $4f$ states. This leads us to conclude the existence of two different Bi states in Ag_2BiO_3 , both close in energy to Bi^{3+} [15].

K_α source (photon energy, 1486.6 eV). The base pressure during XPS was in the low 10^{-10} mbar range. The spectra were collected using an analyzer pass energy of 20 eV. XPS spectra were analyzed using the CASAXPS software. The charge neutralizer was used, and the C $1s$ was set to 284.8 eV for binding energy calibration [12,13]. To fit the peaks, a combination of multiple Gaussian-Lorentzian mixture functions and a Shirley background was used. The binding energy separation and the area ratio of the doublets were not constrained, but the results are within experimental error of the tabulated values [14]. The sum of all the fitted functions to XPS peaks is shown with a black curve in Fig. 2.

Optical spectroscopic ellipsometry measurements were performed using a variable-angle spectroscopic ellipsometer (VASE, Woollam) with photon energy in the range of 0.7–6.5 eV at incident angles of 70° . The real and imaginary parts of the dielectric function can be obtained accurately from the ellipsometric angles $\psi(\omega)$ and $\Delta(\omega)$ extracted from the optical spectra, without the need of a Kramers-Kronig analysis.

The Raman data were collected in backscattering geometry using a Dilor XY triple-grating Raman spectrometer equipped with a charge-coupled device camera as detector. With power of 0.2 mW at 632 nm it was possible to measure Raman spectra on polished surfaces of the Ag_2BiO_3 samples. Low-temperature Raman measurements were performed between 10 and 300 K. The resolution of our spectrometers for this experiment was about 3 cm^{-1} .

III. COMPUTATIONAL DETAILS

The band structure calculations for Ag_2BiO_3 presented in Fig. 3(d) were obtained using the Vienna *ab initio* simulation package (VASP 5.4) with the generalized gradient approximation (GGA) of Perdew-Burke-Ernzerhof (PBE) type exchange-correlation potential [16]. The cutoff energy of the plane-wave basis set was set to be the maximum cutoff energy (ENMAX) value in the pseudopotential plus 30%. A

centered $3 \times 3 \times 2$ Monkhorst-Pack grid was used for the self-consistent field (SCF) calculations.

The electronic structure calculations shown in Figs. 4(a)–4(d) were performed using DFT with the full-potential linearized-augmented-plane-wave code WIEN2K [17]. Exchange and correlation effects were treated within the local density approximation (LDA) [18]. For Ag_2BiO_3 , we use the $Pnn2$ unit cell with the lattice constants $a = 5.983 \text{ \AA}$, $b = 6.324 \text{ \AA}$, and $c = 9.576 \text{ \AA}$, as determined in Ref. [10]. For BaBiO_3 , we use the $P2_1/n$ unit cell with the lattice constants $a = 6.174 \text{ \AA}$, $b = 6.125 \text{ \AA}$, and $c = 8.652 \text{ \AA}$, as determined in Ref. [19]. For both bismuthates, a $6 \times 6 \times 4$ k -point grid was used for the Brillouin-zone integration. Projections onto oxygen molecular orbitals were performed with a modified version of WIEN2K, following the procedure outlined in Ref. [20].

IV. RESULTS AND DISCUSSION

A. Analysis of XRD, XPS, and XAS

We used XRD, XPS, and XAS measurements to demonstrate that Ag_2BiO_3 in the $Pnn2$ phase is a bond disproportionated bismuthate. As it is difficult to distinguish the $Pnna$ structure from the $Pnn2$ structure with only powder XRD data, as demonstrated in Fig. 1, we will start by accepting the reported $Pnn2$ phase reported and assess the consistency of various properties we measure with this structure. The lower scattering power of oxygen in x-ray diffraction and natural twinning of Ag_2BiO_3 crystals make it difficult to discern the $Pnn2$ from the $Pnna$ structure. A previous study on Ag_2BiO_3 using powder neutron diffraction, which is more sensitive to diffraction from oxygen than x rays, resulted in a precise refinement of O atomic positions and a structure where Bi has two distinct sites [10]. We compare the simulated powder XRD and neutron diffraction patterns in Fig. S1 of the Supplemental Material to demonstrate how the $Pnn2$ phase can be identified in neutron diffraction [21].

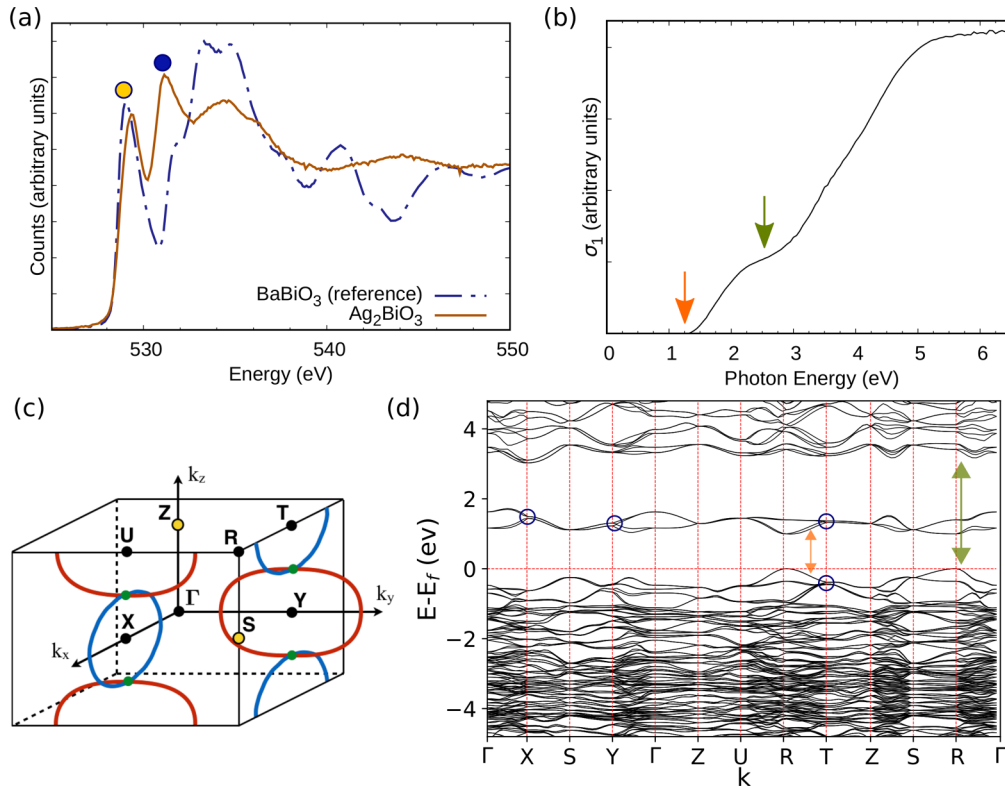


FIG. 3. (a) The x-ray absorption spectra at the oxygen *K* edge of Ag₂BiO₃ and a reference sample of BaBiO₃. (b) Optical spectroscopy data on Ag₂BiO₃ extracted from ellipsometry measurement. (c) Brillouin zone of Ag₂BiO₃ with the high-symmetry points indicated by black dots. The nodal chains are schematically illustrated by the blue and red lines. At the Z and S points (yellow) there are fourfold degeneracies, formed by two Weyl points with opposite chirality. (d) Band structure of Ag₂BiO₃ in the *Pnn2* phase using DFT calculation with hybrid functionals.

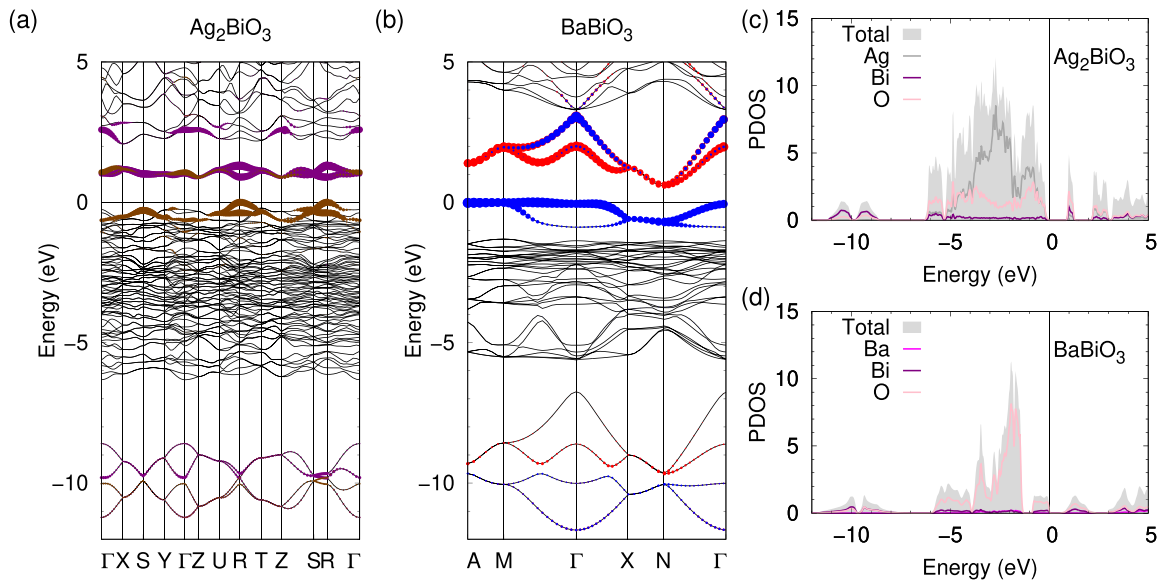


FIG. 4. (a) The DFT (LDA) band structures of Ag₂BiO₃ in the *Pnn2* phase. The contributions from the O *a*_{1g} molecular orbital of the small (purple) and large (brown) octahedra are represented with fat bands. The colors for octahedra match the Ag₂BiO₃ unit cell presented in Fig. 1(c). (b) The band structures of BaBiO₃ in the *P2₁/n* phase. The contributions from the O *a*_{1g} molecular orbital of the small (red) and large (blue) octahedra are represented with fat bands. The colors for octahedra match the BaBiO₃ unit cell presented in Fig. 1(e). (c) Partial density of states (PDOS) of Ag₂BiO₃, showing the contribution from Ag, Bi, and O. (d) PDOS of BaBiO₃, showing the contribution of Ba, Bi, and O.

In the $Pnn2$ phase, Ag_2BiO_3 has two distinct bismuth sites resulting in two BiO_6 octahedra with shorter and longer Bi-O bonds. It should be emphasized that the Bi-O distances vary within each of the two types of octahedra in Ag_2BiO_3 . These Bi- O_6 octahedra are edge sharing along the a direction but only share corners along the b and c directions. The O-O distances at the shared edges of these octahedra are shorter than the distances between the other oxygen atoms, which may correspond to oxygen dimerization at the shared edges. The Ag atoms are sitting between the BiO_6 octahedra channels and are bonded to three oxygen atoms each. The shortest Ag-O distances for both Ag sites are 2.1464 and 2.2065 Å, which are expected for Ag^{1+} typically seen in oxides.

The x-ray photoelectron spectra for Ag, Bi, and O in Ag_2BiO_3 are presented in Figs. 2(a)–2(c). As expected, only one state is observed for Ag, with peak centers at 373.8 eV [peak D1 in Fig. 2(b)] and 367.8 eV [peak D2 in Fig. 2(b)] which match the transition seen in Ag^{1+} in other oxides and chalcogenides [14]. The splitting here is expected for the d states due to spin-orbit coupling (SOC). The XPS of O shows three peaks at 529.1 eV (C), 530.8 eV (B), and 532.6 eV (A). As for the minor peak at 532.6 eV [peak A in Fig. 2(a)], it was attributed to surface contaminants in other bismuthates [22], and such contaminants may be present on the surface of our samples. The binding energy of the main peak for O 1s at 529.1 eV [peak C in Fig. 2(a)] is comparable to the binding energy of O 1s in BaBiO_3 [22]. XPS shows evidence for KOH on the surface of the sample as evidenced by an observed K peak [shown in Supplemental Fig. S2(a)]; we cannot rule out that some of the intensity at 530.8 eV originates from KOH [23] [peak B in Fig. 2(a)]. Furthermore, contamination such as carbonates, which were also observed in the C 1s spectrum [see Supplemental Fig. S2(a)], might also contribute peak B. However, analyzing the relative amount of potassium and carbonate contaminations, peak B cannot be purely due to those contaminations; see Table I of the Supplemental Material. Considering that the area of the fitted curve at 530.8 eV is comparable to the area of the main peak at 529.1 eV (Table I of the Supplemental Material), we expect the signal to originate from a similar amount of oxygen atoms on the surface of the Ag_2BiO_3 samples. Looking at the different O-O and Bi-O distance for oxygen atoms at the shared edges and corners of the BiO_6 octahedra, we propose that the peaks at 530.8 and 529.1 eV may originate from different states in the oxygen atoms at the shared corners and the shared edges of the BiO_6 octahedra.

Assigning distinct oxygen atoms as the origin for the different XPS peaks, the peak at 529.1 eV may originate from the dimerized oxygen at the shared edges of the octahedra with a bond length of 2.6588 Å, while the contribution to the peak at 530.8 eV from Ag_2BiO_3 likely comes from the corner-shared oxygens. Another possibility is that the different oxygen states at 529.1 and 530.8 eV arise from the interaction of the oxygen atoms with silver atoms at different distances, where the oxygen atoms at the shared corners of the octahedra are farther away from the nearest silver atoms, while the oxygen atoms at the shared edges are closer to silver atoms. If all oxygen atoms in Ag_2BiO_3 have equivalent Bi-O interaction, then the electronic origin for the split peaks at 529.1 and 530.8 eV

depends on the extent of the O 1s core-hole potential and the Bi 6s/O 2p hybridization [22].

The Bi 4f spectra, shown in Fig. 2(c), support the presence of two Bi states in this compound, and these states have similar binding energy (158.0 eV for peak G2 and 158.5 eV for peak F2). The ratio of the areas of the two peaks is nearly 1:1, suggesting that the two different Bi states are due to the two distinct Bi atoms in the unit cell. It might be possible that one of the Bi states is due to surface contaminations such as hydroxides or carbonates. However, this would imply that the 1:1 ratio of the two Bi states observed is mere coincidence. Furthermore, if one of the components were due to contamination, the amount of Bi would be too little compared with the Ag amount (see Table I of the Supplemental Material). For now, we consider the two Bi peaks observed as originating from Ag_2BiO_3 . Comparing the measured binding energies with those for Bi^{5+} , as in NaBiO_3 [24], and Bi^{3+} , as in Bi_2O_3 [15], we realize that both are close to the value for Bi^{3+} . This might hint that the system is bond disproportionated rather than charge disproportionated. Please note that the Bi 4f binding energies are similar to the one observed in BaBiO_3 [25] but the Bi 4f spectrum for Ag_2BiO_3 shows a clearer asymmetry.

The XPS spectra thus indicate two different Bi sites, consistent with a disproportionated state, and optical conductivity evidence for a band gap (Sec. IV B) supports this interpretation. However, whether Ag_2BiO_3 is charge or bond disproportionated remains unclear without examining the XAS data. XAS results at the oxygen K edge, presented in Fig. 3(a), show a sharp prepeak at 529 eV, which originates from a high hole density in the oxygen p orbitals. This is similar to the results on BaBiO_3 [22]. The higher-energy region at the K edge is clearly different from the BaBiO_3 spectrum, reflecting the different oxygen environment in Ag_2BiO_3 . A second peak is seen in the XAS results of Ag_2BiO_3 , and the two XAS peaks [marked with yellow and blue circles in Fig. 3(a)] are ~ 2 eV apart. This energy difference is similar to peaks B and C in the oxygen XPS spectra.

The combination of corner- and edge-sharing octahedra in Ag_2BiO_3 can contribute to the different XAS spectra above 530 eV. Another peak at 531 eV is seen for Ag_2BiO_3 , and the origin of this peak is the higher-energy states of O in Ag_2BiO_3 . If we compare Figs. 4(c) and 4(d), we see a peak in the oxygen partial density of states at 2 eV in Ag_2BiO_3 that is much less intense than in BaBiO_3 . In the ionic limit, we have $\text{Ag}^{1+} 4d^{10}$, $\text{Bi}^{3+} 6s^2$, and $\text{O}^{2-} 2p^6$ ions making up Ag_2BiO_3 , where the BiO_6 octahedra are made up of either $\text{Bi}^{3+}(6s^2)$ -O bonds that are longer or $\text{Bi}^{3+}(6s^2\bar{L}^2)$ -O bonds that are shorter. The ligand hole pairs (\bar{L}^2) condense on these smaller octahedra, where the O atoms have equal charge on them. The disproportionation leading to the small and large octahedra in this case is described as bond disproportionation.

One is tempted to conclude that there is a similar origin for both of these sets of peaks, such as the difference between oxygen atoms at the shared edges and corners of the BiO_6 octahedra. However, the area under the curve for the XPS peaks is equivalent for B and C. Reconciling the XAS and XPS results, if the oxygen atoms are equivalent in terms of interaction with Bi and the split in the O 1s XPS is electronic in nature, then an oxygen ligand hole will be distributed over six

oxygen atoms in the BiO_6 octahedron. In the case of O 1s, the XPS peak splitting originates from oxygen atoms at different distances to bismuth, which suggests that an oxygen hole may be distributed over four oxygen atoms at the shared edges of the BiO_6 octahedra. The oxygen hole ligand distribution in the octahedra of Ag_2BiO_3 is discussed below in Sec. IV C.

B. Band gap and topology in disproportionated Ag_2BiO_3

The band structure of Ag_2BiO_3 in the $Pnn2$ phase resulting from DFT calculations is presented in Fig. 3(d), where we have a band gap of ~ 1.25 eV resulting from hybridization of O $2p$ bands and the Bi $6s$ band, with antibonding character. The second set of bands above the Fermi level (E_F) is located ~ 3 eV above E_F and corresponds to the unfilled Bi $6p$ bands. The band gap from the optical conductivity measurement is ~ 1.25 eV [the transition between bands is marked with an orange arrow in Fig. 3(b)], which corresponds well with transitions expected in our calculated band structure [marked with an orange arrow in Fig. 3(d)]. The real and imaginary parts of the dielectric constant of Ag_2BiO_3 are shown in Supplemental Fig. S3. The upturn starting at ~ 2.5 eV in the optical conductivity corresponds to transitions from bands below E_F to the empty Bi $6p$ bands in Ag_2BiO_3 , which are marked with green arrows in Figs. 3(b) and 3(d). The consistency between the features seen in our optical conductivity measurement and the expected transitions in our calculated band structure provide further evidence for Ag_2BiO_3 being in the disproportionated $Pnn2$ phase. In the $Pnna$ phase, Ag_2BiO_3 is a semimetal and expected to have a nonzero density of states at the Fermi level [6] and so no gap in the optical conductivity.

We emphasize that the nonsymmorphic space group $Pnn2$ (space group 34) of Ag_2BiO_3 leads to symmetry-enforced nodal loops in all bands, i.e., twofold Weyl crossings along 1D loops. These nodal loops are protected by the glide mirror symmetries $\{m_{010}|\frac{1}{2}\frac{1}{2}\frac{1}{2}\}$ and $\{m_{100}|\frac{1}{2}\frac{1}{2}\frac{1}{2}\}$ and touch each other on the intersection lines of the mirror planes, thereby forming “nodal chains” [26–28]; see Fig. 3(c). These Weyl nodal lines carry a nontrivial π -Berry phase, leading to drumhead surface states. The Weyl nodal-chain feature is not removable by perturbations as long as the glide mirror symmetries are preserved. In our band calculations of Fig. 3(d) these Weyl nodal chains are seen in various bands as crossing points close to high-symmetry points (see, e.g., crossings marked by blue circles close to the X, Y, and T points). To access the anomalous magnetotransport properties of the nodal chains [26], we may be tempted to use chemical doping to shift the Fermi level and approach these band crossings. However, if the chemical doping changes the $Pnn2$ symmetry, then these topological features may be annihilated. In addition, we note that at the S and Z points the bands form fourfold degeneracies, composed of two Weyl points with opposite chirality [yellow dots in Fig. 3(c)].

Including hybrid functionals in our calculations results in an increase in the band gap for Ag_2BiO_3 in comparison with calculations in the literature [6] with a direct gap of ~ 1.0 eV at the R point in the band structure. However, this value remains slightly lower than the experimentally estimated value of ~ 1.25 eV from our optical conductivity measurement. This may be limited by the optically active transitions in Ag_2BiO_3

that do not correspond to the lowest band gap in our band structure or the inadequacy of the band calculations in providing accurate band-gap values even with hybrid functionals. Ag_2BiO_3 in the $Pnn2$ is predicted to be a good photovoltaic material [29], and our results clarifying the band gap experimentally are an important step forward. The ~ 1.25 -eV band gap in Ag_2BiO_3 falls within the 1.1–1.45-eV range where maximum efficiency is expected for single-junction solar cells [30]. XPS results, shown in Supplemental Fig. S2(b), suggest that the valence band is ~ 0.9 eV below the Fermi level, and this shows promise for introducing in-gap states in Ag_2BiO_3 . In future studies, we will need to examine the stability of Ag_2BiO_3 when exposed to different levels of radiation to assess its potential in photovoltaic applications.

C. Comparing Ag_2BiO_3 and BaBiO_3

Next, we would like to highlight the extent of similarity and some of the differences between Ag_2BiO_3 and BaBiO_3 . Both materials have a bulk band gap due to disproportionation of “ Bi^{4+} ,” but the octahedra are only corner sharing in BaBiO_3 while the octahedra are sharing edges and corners in Ag_2BiO_3 . The nominal Bi^{4+} oxidation state that leads to the disproportionated charge or bonds in these compounds is achieved through a different number of atoms. While having one Bi atom and three oxygen atoms, it takes two monovalent Ag^{1+} ions or one divalent Ba^{2+} ion to achieve the same average formal charge of 4+ for Bi. Thus $(\text{Ag}^{1+})_2(\text{Bi}^{4+})(\text{O}^{2-})_3$ and $(\text{Ba}^{2+})(\text{Bi}^{4+})(\text{O}^{2-})_3$ have the same unstable average formal charge for Bi in different crystal structures and lead to disproportionation in both Ag_2BiO_3 and BaBiO_3 . However, similar to BaBiO_3 , there is a significant amount of oxygen character in the empty conduction states of Ag_2BiO_3 above the Fermi level. To be more specific, these states are formed by oxygen molecular orbitals with a_{1g} symmetry centered on the *small* BiO_6 octahedra. In Fig. 4(a), they are highlighted as purple fat bands for Ag_2BiO_3 , while in Fig. 4(b), they are highlighted as red fat bands for BaBiO_3 . In the previous theoretical studies on BaBiO_3 [31,32], this situation was referred to as a bipolaronic condensation of oxygen holes. For Ag_2BiO_3 we show in Supplemental Fig. S4 the orbital contribution from Bi s and p in the small and large O_6 octahedral cages, as well as the O $2p$. The significant contribution of O $2p$ above the Fermi level is consistent with a high density of oxygen holes as evidenced by the prepeak in XAS [Fig. 3(a)].

As one can also see in Fig. 4, the valence state within the ~ 1 -eV range below the Fermi level has, in turn, a strong character of O a_{1g} molecular orbitals centered on the *large* BiO_6 octahedra (brown fat bands for Ag_2BiO_3 and blue fat bands for BaBiO_3). Together, these two sets of oxygen molecular orbital states around the Fermi level constitute the antibonding manifold resulting from the strong hybridization between the Bi $6s$ and O a_{1g} orbitals. The latter appears to be as strong in Ag_2BiO_3 as it was found to be in BaBiO_3 , which is evident from the fact that in both systems the bonding combination is pushed down as far as -10 eV. A feature of the Ag_2BiO_3 band structure is the presence of Ag $4d$ bands in the same energy region where the nonbonding oxygen bands are located, from approximately -7 eV up to the Fermi level [shown in Supplemental Fig. S4(a)]. It was demonstrated in BaBiO_3

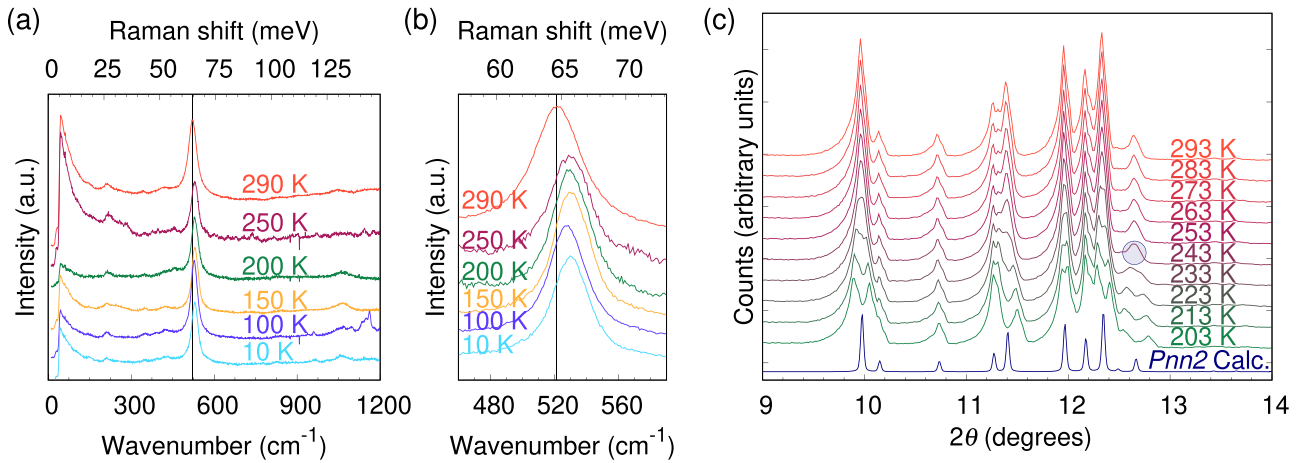


FIG. 5. (a) Raman spectra of Ag_2BiO_3 at different T , between 290 and 10 K. (b) The same Raman spectra in (a), emphasizing the peak at 520 cm^{-1} , characteristic of the breathing mode in disproportionated bismuthates. (c) Powder XRD of Ag_2BiO_3 collected at different T , between 293 and 203 K. The calculated XRD pattern for Ag_2BiO_3 in the $Pnn2$ phase is plotted at the bottom.

that the octahedral angle between Bi-O_6 octahedra effects the Bi-O hybridization [32]. Band calculations in BaBiO_3 with a 0° and 16° octahedral tilting show bands with narrower energy dispersion with increased tilt angle. The conduction band in Ag_2BiO_3 is considerably narrower compared with that in BaBiO_3 , which is probably a result of weaker Bi-O hybridization due to the geometrical arrangement of the BiO_6 octahedra in Ag_2BiO_3 . In Ag_2BiO_3 , the edge-sharing Bi-O_6 octahedra along the a direction and the high angle of 36° between the Bi-O-Bi at the shared corners along the b and c directions contribute to reduced hybridization. This qualitative statement about the hybridization should be confirmed with DFT calculations in future studies. The Ag might play a role in reducing the band gap in Ag_2BiO_3 , as seen in the Ag-containing pyrochlore oxides [33]. This narrowing effect is not clear when we compare Ag_2BiO_3 with BaBiO_3 due to the different crystal structure, but replacing the Ag with another monovalent atom, such as Na_2BiO_3 , can help us to study the effect of Ag. The contribution from Ag bands near the Fermi level is shown in the partial density of states (PDOS) of Ag_2BiO_3 presented in Fig. 4(c). In comparison, the PDOS of BaBiO_3 , shown in Fig. 4(d), has a significant contribution from only Bi and O near the Fermi level and no significant contribution from the Ba.

While in BaBiO_3 we have an indirect band gap as shown in Fig. 4(b), in Ag_2BiO_3 the band gap is direct as shown in Figs. 3(d) and 4(a). The role of the Ag $4d$ bands that extend over a wide energy range below the Fermi level is not clear for now. Identifying the effect of edge-sharing BiO_6 octahedra, crystal symmetry, and Ag bands on the band structure of Ag_2BiO_3 will be an important part of future studies. Future work should include replacing Ag with other monovalent metal M^{+1} atoms, varying the tilting angle of Bi-O_6 octahedra, and studying the lower-symmetry Pn phase.

The Raman spectra of Ag_2BiO_3 have a strong phonon mode at 520 cm^{-1} , shown in Fig. 5, which is similar to the phonon mode observed in pristine BaBiO_3 at 570 cm^{-1} [34]. In the case of BaBiO_3 , the phonon is attributed to the breathing mode originating from local distortion in the bond disproportionated BaBiO_3 , so it is likely that a similar energy

phonon originates from a similar breathing mode accompanying the disproportionation in Ag_2BiO_3 . The slight difference in energies between the phonon modes in Ag_2BiO_3 and BaBiO_3 is due to the different arrangement of the BiO_6 octahedra in the two compounds and the slightly different Bi-O distances. A higher-energy phonon mode originating from higher-harmonic phonon modes can be seen in the Raman spectra of Ag_2BiO_3 at 1100 cm^{-1} , which is similar in value to phonons in the spectra of pristine BaBiO_3 [34].

D. Transition to Pn phase in Ag_2BiO_3

We have closely measured the phonon mode at 520 cm^{-1} as a function of temperature between 290 and 10 K and have observed a shift in the phonon peak position cooling down from 290 to 250 K but no further shift in the phonon mode cooling down to 10 K. We have performed powder XRD measurements on Ag_2BiO_3 at low T and observe a splitting in some peaks at 240 K that corresponds to the monoclinic distortion previously reported [10]. This distortion leads to reduction of symmetry of Ag_2BiO_3 from $Pnn2$ to Pn .

As explained in Sec. IV A, it is difficult to distinguish whether Ag_2BiO_3 crystallizes in the $Pnn2$ or the $Pnna$ phase from XRD alone, and neutron diffraction studies were required to clarify the $Pnn2$ phase at room temperature [10]. The band gap and splitting in the Bi XPS states measured on our samples suggest that Ag_2BiO_3 is indeed in the $Pnn2$ phase. However, the Pn phase of Ag_2BiO_3 is distinct from the higher-symmetry phases and can be identified with XRD. The splitting of the (202) peak at $\sim 12.6^\circ$ for temperatures $< 243\text{ K}$ is highlighted with a blue circle in Fig. 5(c), which results from the reduced symmetry of Ag_2BiO_3 from $Pnn2$ to Pn .

It is likely that the shift in the phonon mode observed in Raman measurements at 250 K is related to the phase transition observed in powder XRD. The transition observed in our samples is consistent with the previously reported phase transition in neutron diffraction measurements on Ag_2BiO_3 [10]. Future studies are needed to investigate the effect of different synthesis conditions on the oxygen content in Ag_2BiO_3 and

whether this influences the distortion in these samples at low T .

Measurements that can be used to probe the band structure of Ag_2BiO_3 such as scanning tunneling spectroscopy or angle-resolved photoemission spectroscopy are typically performed at low temperature. Any properties measured on Ag_2BiO_3 below ~ 250 K are representative of the material in the Pn phase, and the band structure of this phase will be the relevant one for those measurements. Luckily, the Pn (space group 7) symmetry falls into the nonsymmorphic space groups where a single glide mirror symmetry is expected to lead to symmetry-enforced Weyl nodal lines [26–28], albeit not a nodal chain as in the $Pnn2$ phase.

The disproportionation of Ag_2BiO_3 is still prevalent in the Pn phase, which would lead to a band gap much like the $Pnn2$ phase. Repeating the XPS and XAS measurements at temperatures where Ag_2BiO_3 is in the Pn phase will help reveal whether this transition affects the Bi states or the oxygen holes.

V. CONCLUSIONS

We have demonstrated that despite the use of a high pressure of 6 GPa, Ag_2BiO_3 samples crystallize in a structure consistent with the $Pnn2$ phase as evidenced by the XPS data for Bi and the measured band gap. The band gap observed in this paper is consistent with our band calculations, and we demonstrate that Ag_2BiO_3 even in the $Pnn2$ phase is topologically nontrivial and contains Weyl nodal chains in its band structure (~ 0.5 eV below the Fermi level). We observe a phase transition in Ag_2BiO_3 at low temperatures associated with distortion from the $Pnn2$ phase to the Pn phase from our XRD pattern and Raman spectra. Even in the Pn phase,

Ag_2BiO_3 falls into a nonsymmorphic space group, and Weyl nodal-line features are expected.

The XAS spectra of Ag_2BiO_3 suggest the presence of oxygen holes much like BaBiO_3 , which is consistent with Ag_2BiO_3 being a bond disproportionated bismuthate. Despite the different arrangement of BiO_6 octahedra in BaBiO_3 and Ag_2BiO_3 , we observe a phonon mode in the Raman spectra of Ag_2BiO_3 at similar energy associated with the breathing mode of the disproportionated BaBiO_3 . Our results push forward the group of monovalent bismuthates (M^{+1}) $_2\text{BiO}_3$ as a class of bismuthates with interesting topological properties. Doping divalent atoms on the Ag site and performing *in situ* high-pressure experiments may allow us to destabilize the disproportionation in Ag_2BiO_3 and achieve a metallic state and perhaps even superconductivity in this class of materials in analogy to BaBiO_3 . We envision that this work will open up the field of disproportionated oxides beyond those in the perovskite structure.

ACKNOWLEDGMENTS

We thank Frank Falkenberg, Christine Stefani, Sebastian Bette, and Armin Schulz for technical assistance with experiments. We thank Tom Regier for help with XAS measurements. Research described in this paper was performed at the Canadian Light Source, which is supported by the Canada Foundation for Innovation, the Natural Sciences and Engineering Research Council of Canada, the University of Saskatchewan, the Government of Saskatchewan, Western Economic Diversification Canada, the National Research Council Canada, and the Canadian Institutes of Health Research. We thank the Max Planck-UBC-UTokyo Center for Quantum Materials for support.

-
- [1] J. G. Bednorz and K. A. Müller, *Z. Phys. B: Condens. Matter* **64**, 189 (1986).
- [2] L. F. Mattheiss, E. M. Gyorgy, and D. W. Johnson Jr., *Phys. Rev. B* **37**, 3745 (1988).
- [3] S. Seki, X. Yu, S. Ishiwata, and Y. Tokura, *Science* **336**, 198 (2012).
- [4] M. Kargarian and G. A. Fiete, *Phys. Rev. Lett.* **110**, 156403 (2013).
- [5] S. Ishiwata, T. Nakajima, J. H. Kim, D. S. Inosov, N. Kanazawa, J. S. White, J. L. Gavilano, R. Georgii, K. M. Seemann, G. Brandl, P. Manuel, D. D. Khalyavin, S. Seki, Y. Tokunaga, M. Kinoshita, Y. W. Long, Y. Kaneko, Y. Taguchi, T. Arima, B. Keimer *et al.*, *Phys. Rev. B* **101**, 134406 (2020).
- [6] J. He, D. Di Sante, R. Li, X.-Q. Chen, J. M. Rondinelli, and C. Franchini, *Nat. Commun.* **9**, 492 (2018).
- [7] B. Fu, X. Fan, D. Ma, C.-C. Liu, and Y. Yao, *Phys. Rev. B* **98**, 075146 (2018).
- [8] B. Singh, B. Ghosh, C. Su, H. Lin, A. Agarwal, and A. Bansil, *Phys. Rev. Lett.* **121**, 226401 (2018).
- [9] S. Deibele and M. Jansen, *J. Solid State Chem.* **147**, 117 (1999).
- [10] C. P. Oberndorfer, R. E. Dinnebier, R. M. Ibberson, and M. Jansen, *Solid State Sci.* **8**, 267 (2006).
- [11] N. Quackenbush, J. W. Tashman, J. A. Mundy, S. Sallis, H. Paik, R. Misra, J. A. Moyer, J.-H. Guo, D. A. Fischer, J. C. Woicik, D. A. Muller, D. G. Schlom, and L. F. J. Piper, *Nano Lett.* **13**, 4857 (2013).
- [12] P. Swift, *Surf. Interface Anal.* **4**, 47 (1982).
- [13] T. L. Barr and S. Seal, *J. Vac. Sci. Technol., A* **13**, 1239 (1995).
- [14] J. Moulder and J. Chastain, *Handbook of X-ray Photoelectron Spectroscopy: A Reference Book of Standard Spectra for Identification and Interpretation of XPS Data* (Physical Electronics Division, Perkin-Elmer, Eden Prairie, MN, 1992).
- [15] M. S. Hegde, P. Barboux, C. C. Chang, J. M. Tarascon, T. Venkatesan, X. D. Wu, and A. Inam, *Phys. Rev. B* **39**, 4752 (1989).
- [16] J. P. Perdew, K. Burke, and Y. Wang, *Phys. Rev. B* **54**, 16533 (1996).
- [17] P. Blaha, K. Schwarz, G. K. H. Madsen, D. Kvasnicka, J. Luitz, R. Laskowski, F. Tran, and L. D. Marks, WIEN2k: An augmented plane wave plus local orbitals program for calculating crystal properties, Vienna University of Technology (2001).
- [18] J. P. Perdew and Y. Wang, *Phys. Rev. B* **45**, 13244 (1992).
- [19] B. J. Kennedy, C. J. Howard, K. S. Knight, Z. Zhang, and Q. Zhou, *Acta Crystallogr., Sect. B: Struct. Sci.* **62**, 537 (2006).

- [20] K. Foyevtsova and G. Sawatzky, *J. Mod. Phys.* **10**, 953 (2019).
- [21] See Supplemental Material at <http://link.aps.org/supplemental/10.1103/PhysRevMaterials.5.064202> for diffraction simulation, supplemental XPS results, dielectric constant from ellipsometry measurement, and supporting band structure calculations.
- [22] S. Balandeh, R. J. Green, K. Foyevtsova, S. Chi, O. Foyevtsov, F. Li, and G. A. Sawatzky, *Phys. Rev. B* **96**, 165127 (2017).
- [23] M. Favaro, B. Jeong, P. N. Ross, J. Yano, Z. Hussain, Z. Liu, and E. J. Crumlin, *Nat. Commun.* **7**, 12695 (2016).
- [24] G. Kulkarni, V. Vijayakrishnan, G. Ranga Rao, R. Seshadri, and C. Rao, *Appl. Phys. Lett.* **57**, 1823 (1990).
- [25] N. C. Plumb, D. J. Gawryluk, Y. Wang, Z. Ristic, J. Park, B. Q. Lv, Z. Wang, C. E. Matt, N. Xu, T. Shang, K. Conder, J. Mesot, S. Johnston, M. Shi, and M. Radovic, *Phys. Rev. Lett.* **117**, 037002 (2016).
- [26] T. Bzdušek, Q. Wu, A. Rüegg, M. Sigrist, and A. A. Soluyanov, *Nature (London)* **538**, 75 (2016).
- [27] Y.-H. Chan, B. Kilic, M. M. Hirschmann, C.-K. Chiu, L. M. Schoop, D. G. Joshi, and A. P. Schnyder, *Phys. Rev. Materials* **3**, 124204 (2019).
- [28] M. M. Hirschmann, A. Leonhardt, B. Kilic, D. H. Fabini, and A. P. Schnyder, *Phys. Rev. Materials* **5**, 054202 (2021).
- [29] D. H. Fabini, M. Koerner, and R. Seshadri, *Chem. Mater.* **31**, 1561 (2019).
- [30] T. Kirchartz and U. Rau, *Adv. Energy Mater.* **8**, 1703385 (2018).
- [31] K. Foyevtsova, A. Khazraie, I. Elfimov, and G. A. Sawatzky, *Phys. Rev. B* **91**, 121114(R) (2015).
- [32] A. Khazraie, K. Foyevtsova, I. Elfimov, and G. A. Sawatzky, *Phys. Rev. B* **97**, 075103 (2018).
- [33] H. Mizoguchi and P. M. Woodward, *Chem. Mater.* **16**, 5233 (2004).
- [34] S. Tajima, M. Yoshida, N. Koshizuka, H. Sato, and S. Uchida, *Phys. Rev. B* **46**, 1232 (1992).